J. Neurovirol. (2011) 17:455–468
DOI 10.1007/s13365-011-0047-0

Growth-associated protein-43 and ephrin B3 induction in the brain of adult SIV-infected rhesus macaques

Susan V. Westmoreland · Lakshmanan Annamalai · Margaret R. Lentz · Eva-Marie Ratai · Basel Assaf · Karen Boisvert · Thanhthao Huynh · Eric J. Vallender · Gregory M. Miller · Bertha K. Madras · R. Gilberto Gonzalez

Received: 23 November 2010 / Revised: 6 June 2011 / Accepted: 12 July 2011 / Published online: 26 July 2011

Abstract Understanding the mechanisms of neuronal regeneration and repair in the adult central nervous system is a vital area of research. Using a rhesus lentiviral encephalitis model, we sought to determine whether recovery of neuronal metabolism after injury coincides with the induction of two important markers of synaptodendritic repair: growth-associated protein-43 (GAP-43) and ephrin B3. We examined whether the improvement of neuronal metabolism with combined anti-retroviral therapy (cART) after simian immunodeficiency virus (SIV) infection in rhesus macaques involved induction of GAP-43, also known as neuromodulin, and ephrin B3, both implicated in axonal pathfinding during neurodevelopment and regulation of synapse formation, neuronal plasticity, and repair in adult brain. We utilized magnetic resonance spectroscopy to demonstrate improved neuronal metabolism in vivo in adult SIV-infected cART animals compared to untreated and uninfected controls. We then assessed levels of GAP-43, ephrin B3, and synaptophysin, a presynaptic marker, in three brain regions important for cognitive function, cortex, hippocampus, and putamen, by quantitative real-time RT-PCR and immunohistochemistry. Here we demonstrate that (1) GAP-43 mRNA and protein are induced with SIV infection, (2) GAP-43 protein is higher in the hippocampus outer molecular layer in SIV-infected animals that received cART compared to those that did not, and (3) activated microglia and infiltrating SIV-infected macrophages express abundant ephrin B3, an important axonal guidance molecule. We propose a model whereby SIV infection triggers events that lead to induction of GAP-43 and ephrin B3, and that short-term cART results in increased magnitude of repair mechanisms especially in the hippocampus, a region known for high levels of adult plasticity.

Keywords Rhesus · Macaque · SIV · GAP-43 · Ephrin B3 · Neuronal injury · Synaptophysin · Plasticity · Microglia

S. V. Westmoreland (✉) · L. Annamalai · B. Assaf · K. Boisvert
Division of Comparative Pathology, New England Primate Research Center, Harvard Medical School,
Southborough, MA 01772, USA
e-mail: Susan_westmoreland@hms.harvard.edu

E. J. Vallender · G. M. Miller · B. K. Madras
Division of Neuroscience, New England Primate Research Center, Harvard Medical School,
Southborough, MA, USA

T. Huynh
Tufts Cummings School of Veterinary Medicine,
North Grafton, MA, USA

M. R. Lentz · E.-M. Ratai · R. G. Gonzalez
A.A. Martinos Center for Biomedical Imaging and Neuroradiology Division, Massachusetts General Hospital,
149 13th St,
Charlestown, MA, USA

Present Address:
L. Annamalai
Oregon Primate Research Center,
Beaverton, OR, USA

Introduction

In the absence of productive neuronal infection, lentiviral encephalitis causes partially reversible neuronal injury through indirect mechanisms mediated by viral proteins and proinflammatory cytokines largely released by infected infiltrating macrophages and activated microglia. Human immunodeficiency virus (HIV)-infected macrophages and microglia within the central nervous system (CNS) release

neurotoxic agents, including viral proteins (i.e., env, tat) and host inflammatory proteins, which cause synaptodendritic damage, neural dysfunction, and neuronal death (Alirezaei et al. 2007; Bissel et al. 2002; Everall et al. 2002, 2001; Lipton et al. 1995; Westmoreland et al. 1996). SIV-infected rhesus macaques develop encephalitis histologically and pathophysiologically similar to HIV encephalitis (HIVE) with comparable loss of pre- and post-synaptic neuronal processes (Bissel et al. 2002; Masliah et al. 1992a, c, 1997; Wiley et al. 1991), loss or alteration of specific neuronal subpopulations, such as parvalbumin-positive interneurons (Masliah et al. 1992b), alterations in calmodulin-dependent kinase II (CaMKII) activation (Gupta et al. 2010), and increased neuronal apoptosis (Alirezaei et al. 2007; Bissel et al. 2002; Everall et al. 2002, 2001; Lipton et al. 1995; Westmoreland et al. 1996). Consequently, the SIV-infected rhesus provides an important model to evaluate mechanisms of neuronal injury and repair. Using brain magnetic resonance spectroscopy (MRS), we have demonstrated significant decreases in the neuronal metabolism marker *N*-acetylaspartate (NAA) in SIV-infected rhesus consistent with neuronal injury and loss (Gonzalez et al. 2000; Greco et al. 2004; Lentz et al. 2005; Lentz et al. 2008). We have also demonstrated that the magnitude of NAA decrease (expressed as a ratio of stable creatine, NAA/Cr) with SIV infection correlates statistically with the severity of encephalitis and the structural synaptodendritic alterations evidenced by reduced immunohistochemical expression of synaptophysin (SYN) (Gonzalez et al. 2000; Lentz et al. 2008; Williams et al. 2005).

Reversal of HIV-associated neuronal injury is challenging, as adult CNS neurons are largely unable to regenerate or regrow axons once injured. Nevertheless, HIV patients suffering from AIDS dementia complex improve clinically when treated with highly active anti-retroviral therapy (HAART) indicating that some of the functional impairment in neurons is reversible. The mechanisms of this clinical improvement are largely unknown.

Neurons in the adult brain have intrinsic adaptive and repair capabilities, which manifest as local axonal sprouting, reshaping of dendritic morphology, remodeling of neuronal circuitry, and region-specific neurogenesis. In the adult brain, accumulating evidence indicates that genes/proteins critical for neuronal development, such as GAP-43 and ephrin B3, are also implicated in processes of neuroadaptation and neuronal repair. GAP-43, a neural-specific calmodulin and actin-binding protein expressed at high concentrations in pre-synaptic membranes (Strittmatter et al. 1992), was first identified as a contributor to neurite outgrowth in neurogenesis (Jacobson et al. 1986). Found at high levels in growth cones and immature synapses when neuronal connections are first established (Benowitz et al.), GAP-43 transduces intra- and extracellular signals to regulate cytoskeletal organization in the synapse terminal (Benowitz and Routtenberg 1997). Cumulating evidence implicates GAP-43 in promoting regeneration and repair (Benowitz et al. 1988, 1989, 1990a; Neve et al. 1988). Gene expression profiles after stroke injury have revealed upregulation of several genes critical in neurodevelopment, including GAP-43 (Carmichael et al. 2005; Perrone-Bizzozero et al. 1988). Upregulation of GAP-43 is also implicated in neuronal repair and functional recovery of the cerebral cortex following spinal cord injury in macaques (Higo et al. 2009).

Ephs, a family of receptors, and ephrins, their respective ligands, function as axonal guidance molecules during neurodevelopment and are implicated in neurogenesis, synaptic plasticity, and neuronal repair in the adult brain. Specifically, the ligand ephrin B3 promotes neurogenesis in the hippocampus, and paradoxically acts as a repellant in vertebrate embryonic axonal pathfinding (Benson et al. 2005; Chumley et al. 2007). In murine hippocampal mossy fiber axons during development, ephrin B3 functions through reverse signaling as a repulsive guidance receptor to mediate pruning of axons by promoting retraction of growth cones (Xu and Henkemeyer 2009), but postnatal rodent studies suggest that axonal responses to ephrin B3/ephB3 signaling pathways may switch from inhibition to growth promotion (Liu et al. 2006). Ephrin B3 also functions as an anti-apoptotic agent to reduce neuronal cell death during neurogenesis (Furne et al. 2009). Intriguingly, GAP-43 induction in injured neurons has been associated with activation of the ephrin B3/ephB3 pathway (Liu et al. 2006).

Here, we investigated the potential of the adult nonhuman primate brain to activate regenerative processes in response to lentiviral infection using the SIV-infected, CD8+ cell-depleted accelerated model of HIVE. We have previously presented longitudinal data from eight SIV-infected rhesus macaques demonstrating reversal of SIV-induced NAA/Cr decline in brain due to short-term cART, and associated that reversal with reduction in viral loads in plasma and within activated circulating monocytes, the target cells that traffic virus into the brain (Williams et al. 2005). We have also published that CD8-depletion alone does not significantly alter neural or glial metabolites (Ratai et al. 2011). In this study, synaptodendritic plasticity and neuronal repair in adult rhesus macaques were examined with a specific focus on whether SIV infection and/or cART alter GAP-43 and ephrin B3 expression in the brain. We discovered that GAP-43 is induced in the brain of rhesus infected with SIV, and that GAP-43 protein expression in the hippocampal outer molecular layer (OML) is significantly higher in SIV-infected macaques treated with short-term cART. We also determined that ephrin B3, a regulator of axonal growth, is expressed by activated macrophages and microglia in SIV-

infected rhesus brain. Our results demonstrate that during SIV infection and cART there is induction of proteins implicated in endogenous neuronal repair mechanisms in vivo in the adult primate brain, and that short-term cART contributes to increases in GAP-43 within the hippocampal OML, fibers important in learning and memory.

Materials and methods

Animal inoculation and cART treatment

Eight Indian-origin adult rhesus macaques, housed according to the standards of the American Association for Accreditation of Laboratory Animal Care, were inoculated with SIVmac251 (20ng SIV *p27*, i.v. supplied by Ron Desrosiers, Harvard Medical School) and depleted of $CD8^+$ cells by treatment with the monoclonal anti-CD8 antibody cM-T807 (supplied by Keith Reimann, National Cell Culture Center) on 6, 8, and 12 days post-inoculation (dpi) as previously described to accelerate disease progression (Ratai et al. 2010; Schmitz et al. 1999; Williams et al. 2005). Four of the monkeys also received cART consisting of daily Racivir (RCV, 10 mg/kg, supplied by Raymond Schinazi) and (R)-9-(2-phosphonylmethoxypropyl) adenine (PMPA, 20 mg/kg, Gilead Sciences, Foster City, CA), nucleoside and nucleotide analogs, respectively, neither of which penetrates the CNS (Haworth et al. 1998; Schinazi et al. 1992) (Table 1). The drugs were given orally for 4 weeks beginning on 28 dpi. Terminal cerebrospinal fluid (CSF) samples were analyzed for the presence of RCV metabolites to test for CNS penetration of this drug (Williams et al. 2005).

In vivo MRI and MRS

The eight macaques were analyzed in vivo by MRI and proton magnetic resonance spectroscopy (Table 1). Animals were anesthetized and scanned before and every 2 weeks after SIV inoculation using a clinical 1.5 Tesla General Electric Signa scanner (Milwaukee, WI) using a linear extremity coil as previously described (Williams et al. 2005). Pre-infection scan data from each animal were used as uninfected, non-depleted controls for the study and compared to terminal scan data performed 1–2 days prior to euthanasia. In addition, MRS data from four uninfected controls were used from an earlier study. Uninfected CD8-depleted controls (n=4) were scanned later on a 7.0 Tesla scanner (Erlangen, Germany). Briefly, neuroimaging consisted of T1-weighted sagittal images and T2-weighted axial images. Magnetic resonance spectroscopy was performed on three $1.5\times1.5\times1.5$ cm^3 (3.4 cm^3) voxel regions including frontal cortex (gray and white matter), putamen, and centrum semiovale as previously described (Williams et al. 2005). MR spectra were processed with the SAGE spectral analysis program (General Electric) to quantify resonances of *N*-acetylaspartate, choline (Cho), myoinositol (MI), and creatine (Cr). MRS data confirmed significant decreases in NAA/Cr in animals with SIV infection before cART was initiated. Results were compared with CD8-depleted, uninfected controls (n=4), when possible, and age-matched uninfected rhesus monkeys (n=6; Table 1).

Immunohistochemistry

Details of antibodies used in this portion of the study are included in Table 2. The affinity-purified IgG anti-rat GAP-43 sheep antibody and the immunohistochemistry (IHC) protocol were gifts courtesy of Dr. Larry Benowitz, Children's Hospital, Boston. Rhesus brain tissues were collected fresh at necropsy and were either fixed in 10% neutral-buffered formalin or embedded in OCT compound (Tissue Tek, Sakura Finetek, Torrance, CA), frozen in 2-methylbutane on dry ice, and then stored at −80°C. Five-micrometer cryosections of frontal cortex (FC), hippocampus (HI), and putamen (PUT) were incubated with anti-GAP-43 antibody as previously described (Benowitz et al. 1989, 1990b). Briefly, frozen brain sections were fixed in 2% paraformaldehyde for 15 min on ice. Endogenous peroxidase was blocked by treatment with methanol H_2O_2 followed by 10% normal rabbit serum block. Slides were incubated for 2 h at room temperature with sheep anti-GAP-43 (1:1,000 dilution), washed, then incubated with biotinylated rabbit anti-sheep secondary antibody (1:250). Sections were detected with ABC Standard avidin–biotin peroxidase complex (Vector Laboratories, Burlingame, CA) and 3,3′ diaminobenzidine (DAB) as the chromogen (Dako). Each GAP-43 IHC assay contained slides from three to four uninfected animals as experimental controls and cortex from infant rhesus as positive control for the assay. Negative controls consisted of adjacent sections incubated with isotype-, species-, and concentration-matched irrelevant control antibodies.

Immunohistochemical detection of SYN, macrophage-marker Iba-1, and ephrin B3 were performed on formalin-fixed paraffin embedded brain tissues using the avidin–biotin–horseradish peroxidase complex (ABC) detection method (Vector Laboratories, Burlingame, CA), as previously described (Westmoreland et al. 2002). Briefly, 5-μm brain sections were deparaffinized and rehydrated, and antigen retrieval was accomplished by microwaving in citrate buffer for 20 min. Sections were blocked for non-specific protein binding, and incubated with one of the following primary antibodies diluted in antibody diluent (Dako Corp., Carpinteria, CA): mouse anti-human synaptophysin (Dako, 1:50 dilution, overnight at 4°C), rabbit

Table 1 Cohort of adult rhesus macaques tested for GAP-43 protein and mRNA by immunohistochemitstry and real-time RT-PCR

Number	Designation	Inoculum	CD8 depl	Anti-viral	Surv (days)
1	SIV 1[a,b]	SIVmac251	Yes	No	57
2	SIV 2[a,b]	SIVmac251	Yes	No	63
3	SIV 3[a,b]	SIVmac251	Yes	No	70
4	SIV 4[a,b]	SIVmac251	Yes	No	85
5	SIV cART 1[a,b]	SIVmac251	Yes	Yes	57
6	SIV cART 2[a,b]	SIVmac251	Yes	Yes	57
7	SIV cART 3[a,b]	SIVmac251	Yes	Yes	56
8	SIV cART 4[a,b]	SIVmac251	Yes	Yes	56
9	CD8-depl contr 1[a]	NA	Yes	No	57
10	CD8-depl contr 2[a]	NA	Yes	No	57
11	CD8-depl contr 3[a]	NA	Yes	No	57
12	CD8-depl contr 4[a]	NA	Yes	No	57
13	Control 1[a,b]	NA	No	No	NA
14	Control 2[a,b]	NA	No	No	NA
15	Control 3[·b]	NA	No	No	NA
16	Control 4[·b]	NA	No	No	NA
17	Control 5[·b]	NA	No	No	NA
18	Control 6[·b]	NA	No	No	NA

[a] Denotes frozen tissues analyzed by real-time PCR

[b] Denotes tissues available for immunohistochemistry

anti-human Iba-1 (Wako Pure Chemicals Industries, Richmond, VA, 1:1,000, dilution for 30 min at RT), or rabbit anti-human ephrin B3 (Abcam, Cambridge, MA, 1:100 dilution for 30 min at RT). Tissues were incubated with either biotinylated horse anti-mouse antibody (for synaptophysin) or biotinylated goat anti-rabbit antibody (for Iba-1 and ephrin B3) followed by 30 min incubation with ABC Elite tertiary reagent (Vector). Immunoreactive product was localized with the chromogen 3, 3′ diaminobenzidine (DAB, Dako). Double labeling of brain tissues with Iba-1 and ephrin B3 was completed by first performing IHC for Iba-1 as described above with development in DAB (Dako), followed by IHC for ephrin B3 using the chromogen Liquid Permanent Red (Dako). Slides were coverslipped with aqueous mounting media (Clear-Mount, Electron Microscopy Sciences, Hatfield, PA).

Levels of GAP-43, SYN, and ephrin B3 were determined by computer-aided image analysis as previously described (Annamalai et al. 2010) with some modifications. Images of tissue sections were captured without manipulation using a Q color Olympus camera at ×80 magnification interfaced with Q Capture on a Macintosh Power G5 computer and analyzed using NIH Image J software. Photomicrographs were taken under identical illumination of eight to ten randomly selected, non-overlapping regions from a given region of interest [anterior cingulate gyrus layers 3–5 (ACG), dorsal putamen 9 (PUT), hippocampal inner molecular layer (IML), outer molecular layer (OML), and subiculum from the parahippocampal gyrus]. Ephrin B3 expression was analyzed in cortical white matter avoiding perivascular lesions in order to assess expression in glia rather than infiltrating leukocytes. Individual images

Table 2 Primary antibody source, immunogen, and dilution

Antibody	Source	Catalog no. (lot no.)	Immunogen	Type/format	Dilution
Anti-growth associated protein-43 (GAP-43)	L. Benowitz, Children's Hosp Boston	NA	Entire GAP-43 protein	Polyclonal sheep	1:1,000
Anti-synaptophysin	Dako	M0776 (27760)	Carboxy-terminal cytoplasmic tail of synaptophysin	Monoclonal mouse ascites, IgG1, kappa	1:50
Anti-Iba-1	Wako	019-19741 (NNH3687)	Synthetic peptide corresponding to C terminus of Iba1	Polyclonal rabbit serum	1:1,000
Anti-ephrin B3	Abcam	ab-28388 (now ab-36753) (694107)	Recombinant fragment, corresponding to amino acids 135–341 of human ephrin B3	Polyclonal rabbit serum	1:100

were opened by Image J and the regions of interest (ROI) were drawn manually. Color images were converted to grayscale and nuclei were subtracted from the images using color deconvolution. The ROI was reapplied to the image and the optical density of the ROI was analyzed and expressed as mean density of pixel area. The measure optical density of GAP-43 immunoreactivity of each ROI was transferred into an Excel spreadsheet with eight to ten values generated for each animal and each brain region and expressed as the mean per case and region. Results from infected untreated and cART-treated animals were analyzed and compared to uninfected controls. Tissues from uninfected, CD8-depleted animals were not available for this portion of the study.

Spectral analysis of Iba-1 and ephrin B3 double-labeled slides was performed using an Olympus Vanox S research microscope interfaced with a liquid crystal tunable filter-based camera (CRi, Woburn, MA). Spectral images were obtained for spatial resolution and localization of chromogens (Permanent Red, DAB, and Mayers hematoxylin). Images were automatically acquired from 420 to 720 nm at 20 nm steps and spectral components unmixed. The spectral absorbance of each chromogen was established from single-stain controls and the contribution of each stain calculated from this reference to determine the relative contribution of the stain at each pixel. Individual images were pseudocolorized and then combined into a single image with co-localized signals represented in yellow.

RNA isolation and quantification

Frozen tissues were used to quantify GAP-43 mRNA from the two experimental groups and two control groups of animals: SIV-infected CD8-depleted untreated (n=4), SIV-infected CD8-depleted cART-treated (n=4), CD8-depleted uninfected controls (n=4), and non-CD8-depleted uninfected controls (n=2; Table 1 designated by superscript a). Total RNA was isolated from 75–100 mg of dissected frozen brain specimens (frontal cortex, parietal cortex, putamen, and hippocampus), which had been immediately placed in microcentrifuge tubes with 1 ml of RNAlater (Ambion Biosystems, Austin, TX) and stored at −80°C. These specimens were collected from the same coronal tissue plane as the samples collected and analyzed by MRS and real-time polymerase chain reaction (PCR) and were comparable to the regions analyzed by immunohistochemistry, which were collected from the contralateral hemisphere. Briefly, RNAlater was decanted and tissues were homogenized in 1.5 ml of Trizol reagent (Invitrogen, Carlsbad, CA) using a bead beater and 1 mm diameter silica beads (Biospec Products Inc., Bartlesville, OK). After homogenization, the homogenate was removed to a new tube, 0.2 volumes of chloroform was added, and the aqueous phase was collected after centrifugation at 8,000×g for 5 min at 4°C. The aqueous phase was combined with an equal volume of 70% ethanol, 1 ml of 4 M guanidinium isothiocyanate was added, and the mixture was loaded onto an RNeasy spin column (Qiagen, Valencia, CA). After on-column DNase treatment (Qiagen), the total RNA was eluted in RNase free water, 2 U/μl of recombinant RNase inhibitor (RNasin, Promega Corp., Madison, WI) was added, and the RNA was frozen at −80°C.

The amount of RNA extracted from dissected brain regions was measured using the Quant-iT Ribo Green RNA assay (Invitrogen), adhering to the manufacturer's instructions. Spectrophotometer readings were taken at 260 and 280 nm to assess the quality of RNA isolated and to approximate the RNA concentration in each specimen. For accurate quantification, 20–80 ng of total RNA from each specimen diluted in 100 μl of 1× TAE buffer was loaded into duplicate wells of a 96-well plate and combined with 100 μl of a 1:200 dilution of Ribo Green reagent. After incubating for 10 min at room temperature in the dark, the fluorescence generated in each well was measured for 0.1 s at an excitation and emission of 485 and 535 nm, respectively, using a Victor^3 V 1420 Multilabel Counter (Perkin Elmer, Waltham, MA). Prism 4 software (GraphPad Software Inc., San Diego, CA) was used to calculate the concentration of RNA in each specimen against a standard curve that was generated using known quantities (5–150 ng) of *Escherichia coli* ribosomal RNA.

GAP-43 real-time PCR

Real-time PCR for GAP-43 was performed following protocols described previously with slight modifications (Xie et al. 2007). Briefly, quantification of GAP-43 transcripts in total RNA from dissected brain specimens was conducted using the Roche Universal Probe Library and the Light Cycler 2.0 (Roche Diagnostics). Assays were designed using the Roche Universal Probe Library Assay Design Center. GAP-43 primers, F: ggagaaggcaccactgctac, R: ctttgccgggttcatcag, used probe #36 and RPL13A primers, a control gene, F: gttcggtaccacacgaaggt, R: cacagaaatgccgatggtc, used probe #41. While the primers for RPL13A span introns, the GAP-43 gene contains a single exon gene. For this reason a genomic DNA detector was designed using intronic primers from the tryptophan hydroxylase 2 (TPH2) gene, F: tggaaccctaactaacgtttcg, R: caggtttgtaaccaggcaca, probe #38. All brain specimen cDNAs were confirmed to be free of genomic DNA contamination prior to proceeding with GAP-43 and RPL13A assays.

For each reaction, a Light Cycler TaqMan Master kit (Roche Diagnostics) was used with 10 μM of each primer, 0.2 μl of probe, and either 2 ng of genomic DNA or 50 ng

of cDNA in a total volume of 20 μl. All amplifications were carried out in glass capillary tubes with rapid cycling polymerase chain reaction in a Light Cycler 2.0 instrument under the following conditions: preheat for 1 cycle at 95°C for 15 min; amplification for 45 cycles: 95°C for 10 s, 58°C for 30 s, 72°C for 3 s; and final cooling to 40°C. Genomic DNA was used as a positive control for genomic detector primers.

Statistical analysis of NAA/Cr levels, GAP-43 protein, and mRNA protein expression levels

Nonparametric Mann–Whitney *t* tests were performed for comparison of NAA/Cr MRS data between groups with statistical differences assumed for $p<0.05$. Statistical evaluation of quantitative image analysis data of immunohistochemical assays was performed with GraphPad Prism program. Kruskal–Wallis nonparametric one-way analysis of variance (ANOVA) followed by Dunn's multicomparison test was used to assess statistical differences between groups for each brain region. Statistical differences were assumed for probability values of $p<0.05$ based on post-analysis tests. Analysis of real-time PCR data was done using a modified $\Delta\Delta C_t$ method: $\Delta C_t = C_t(\text{GAP-43}) - C_t(\text{RPL13A})$, $\Delta\Delta C_t = \Delta C_t(\text{experimental}) - \Delta C_t(\text{control})$. In order to facilitate multiple comparisons C_t values were normalized to an arbitrary baseline value of $C_t(\text{RPL13A})=25$. Serial dilutions using whole brain cDNA were used to establish efficiencies for all assays. Fold change was established as $2^{-\Delta\Delta Ct}$. Differences were assumed for probability values of $p<0.05$.

Results

Decrease in neuronal metabolism with acute SIV is partially reversed with cART

To examine the impact of short-term cART on neuronal recovery, eight CD8-depleted and SIV-infected rhesus macaques, four of which received daily oral PMPA and RCV beginning at 28 dpi (each designated by a number in Table 1), were examined longitudinally by in vivo neuroimaging and proton magnetic resonance spectroscopy (1H-MRS) in three brain regions [frontal cortex, centrum semiovale white matter (WM), and basal ganglia] from pre-infection to terminal disease or elected euthanasia. No RCV metabolites were present in the CSF from the treated animals when tested by HPLC (Williams et al. 2005). In SIV-infected rhesus macaques receiving PMPA and RCV, treatment resulted in decreased plasma virus (Williams et al. 2005), decreased virus in the brain compared to untreated/infected controls (Annamalai et al. 2010), and near complete reversal of NAA decline compared to pre-treatment levels (Williams et al. 2005).

Pre-infection in vivo levels of NAA, a marker of neuronal metabolism, relative to the control metabolite creatine, served as control values and were comparable for all animals for each of the three analyzed regions (Fig. 1). Four CD8-depleted, uninfected rhesus were scanned four times over 8 weeks as additional controls, and did not demonstrate significant differences in metabolites compared to pre-infection in the experimental groups (Ratai et al. 2010). The four SIV-infected rhesus macaques developed illness and terminal AIDS with survival between 57 and 85 dpi, while those infected animals that received daily cART, initiated on 28 dpi, were sacrificed at 57 dpi with no clinical signs of AIDS (Table 1). Longitudinal data demonstrated a steady, measurable decrease in pre-treatment NAA/Cr by 27 dpi in all eight infected animals consistent with neuronal injury and metabolic dysfunction in the SIV-infected animals (Williams et al. 2005). Terminally, the cART group exhibited significantly higher mean in vivo NAA/Cr ratios in the FC (Mann–Whitney test, nonparametric, $p=0.0286$, Fig. 1a) and WM (Mann–Whitney test, nonparametric, $p=0.0421$, Fig. 1b) and a trend toward increased NAA/Cr in the basal ganglia at 57 dpi compared with the SIV-infected untreated group (Fig. 1c). There were no significant differences in NAA/Cr between the pre-scans of the three regions in any of the animals nor between the terminal post-scans in the treated animals compared to controls. The full set of *p* values for comparisons of MRS data between groups and for each of the three brain regions examined are summarized in Fig. 1d. Higher neuronal NAA/Cr ratios in treated animals indicates a significant improvement in neuronal metabolism with short-term cART using PMPA and RCV, which do not cross the BBB as previously reported (Fox et al. 2000; Williams et al. 2005).

Synaptic density decreases in cortex and putamen of SIV-infected rhesus with and without cART, but increases in hippocampus

Because GAP-43 is predominantly localized in pre-synaptic membranes, we examined the density of the pre-synaptic vesicle protein synaptophysin in anterior cingulate gyrus, HI [including hilus, granule cell layer (GCL) of the dentate gyrus, and the inner and outer molecular layers (IML, OML)], and putamen. These are regions important for cognitive function and have been associated with HAND. We have previously shown that acute and chronic SIV infection in rhesus macaques causes a significant loss of pre-synaptic terminals reflected by decreases in SYN immunoreactivity in frontal cortex of infected animals compared to uninfected controls, and that these structural pre-synaptic alterations correlate with decreased neuronal metabolism indicated by decreased NAA/Cr MRS ratio in corresponding brain regions (Gonzalez et al. 2000; Williams et al. 2005).

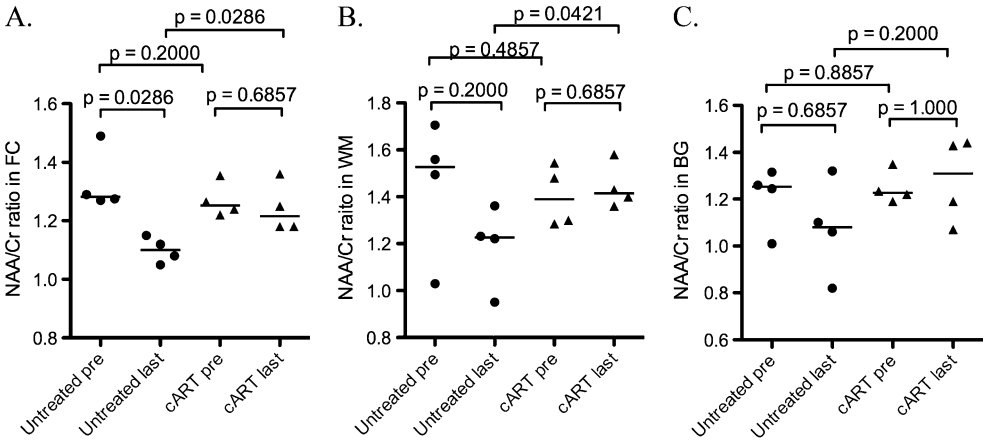

D.

Region	Cohort	Vs. Cohort	p
FC	Untreated pre-infection	Untreated last scan	**0.0286**
	CART pre-infection	CART last scan	0.6857
	Untreated last scan	CART last scan	**0.0286**
WM	Untreated pre-infection	Untreated last scan	0.2000
	CART pre-infection	CART last scan	0.6857
	Untreated last scan	CART last scan	**0.0421**
PUT	Untreated pre-infection	Untreated last scan	0.6857
	CART pre-infection	CART last scan	0.1000
	Untreated last scan	CART last scan	0.2000

Fig. 1 Mean in vivo MRS NAA/Cr levels in the frontal cortex (*FC*, **a**), white matter of centrum semiovale (*WM*, **b**), and basal ganglia (*BG*, **c**) of the untreated (n=4) and cART-treated (n=4) SIV-infected rhesus cohorts from pre-infection and last post-infection scans. Pre-infection and terminal scans revealed significant decline in NAA/Cr in FC in SIV-infected untreated animals (p=0.0286). There were no differences between the pre-infection and terminal scans in the cART-treated animals. **d** NAA/Cr mean values were significantly higher in FC and WM of those animals who received short-term cART (Mann–Whitney t test, p=0.0286 and 0.0421, respectively)

Here, we demonstrate that these SIV-infected rhesus exhibited decreased SYN immunoreactivity in the ACG (Fig. 2a, Kruskal–Wallis, p=0.0345) with a trend toward decreased levels in the PUT (Fig. 2b) and OML (Fig. 2c) compared to uninfected controls. In the hippocampus, there was evidence of a remodeling pattern in response to cART with increased mean levels of SYN in the OML of treated animals (61.86, SD 7.14) compared to mean levels in untreated SIV-infected groups (49.89, SD 6.75; Fig. 2c). Decreased synaptic density persisted in the ACG and PUT despite short-term cART.

GAP-43 protein expression is significantly higher in the outer molecular layer of the hippocampal dentate gyrus in SIV-infected rhesus with cART

Despite decreased pre-synaptic synaptophysin expression observed in cortical ACG, PUT, and HI OML with SIV

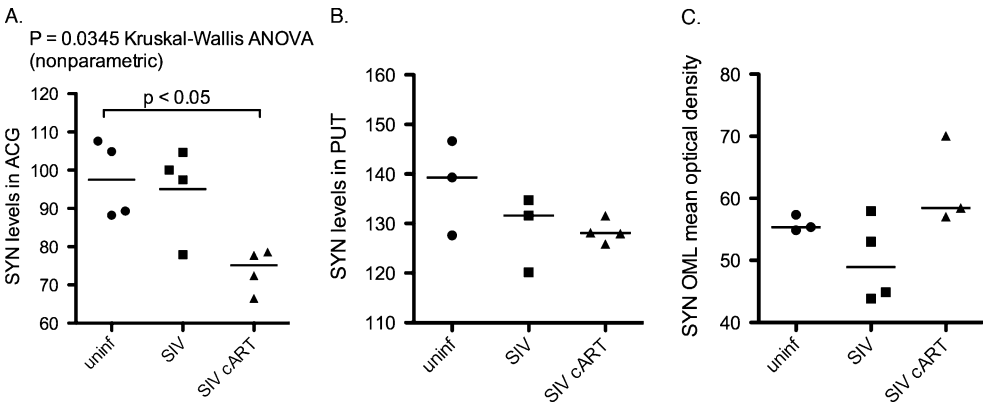

Fig. 2 Computer-aided image analysis of levels of SYN immunoreactivity in anterior cingulate gyrus (*ACG*), dorsal putamen (*PUT*), and hippocampal outer molecular layer (*OML*) in SIV-infected animals with and without cART compared to uninfected controls. Animals infected with SIV had lower SYN levels in ACG, PUT, and HI. SYN levels were higher OML in animals that received short-term cART. Data represent mean levels of SYN in 6–10 non-overlapping areas collected at ×80 magnification

infection described above, mean pre-synaptic GAP-43 protein expression was increased in SIV-infected rhesus in multiple brain regions compared to uninfected controls assessed by immunohistochemistry. In particular, GAP-43 was higher in ACG (Fig. 3b, e) and putamen (Fig. 3k) in SIV-infected rhesus compared to uninfected controls (Fig. 3a, d, j, respectively). Computer-aided image analysis of GAP-43 immunohistochemical levels in the cortical ACG confirmed near significant differences between the three groups of animals (Kruskal–Wallis nonparametric ANOVA, $p=0.0553$, Fig. 4a) with higher GAP-43 expression in SIV-infected rhesus (nonparametric Mann–Whitney, $p=0.0571$) compared to uninfected controls. In addition, GAP-43 expression was higher in SIV-infected untreated rhesus in the PUT (Fig. 3k) compared to controls (Fig. 3j), which was significant (Kruskal–Wallis nonparametric ANOVA, $p=0.0498$, Mann–Whitney post-comparison test $p=0.0286$, Fig. 4b). There was no significant difference in GAP-43 expression in the cortex or PUT between SIV-infected untreated and cART-treated animals (Fig. 4a, b).

GAP-43 expression was significantly higher in the hippocampal OML in animals that received cART (Fig. 3i) compared to uninfected control animals (Fig. 3g), confirmed

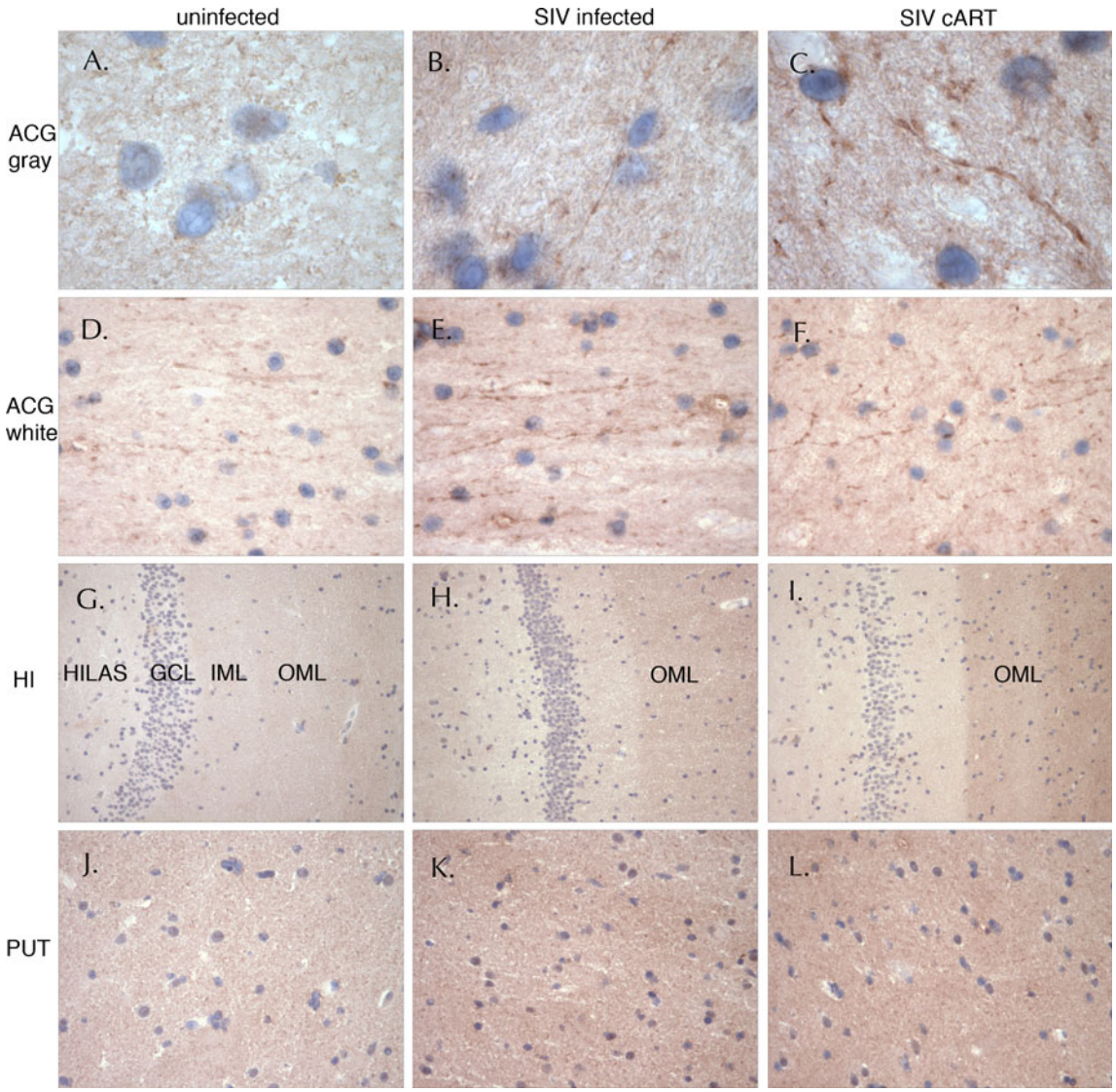

Fig. 3 Composite of GAP-43 immunohistochemistry in anterior cingulate gyrus (*ACG*), hippocampus (*HI*), and putamen (*PUT*) from representative SIV-infected rhesus with and without cART compared to uninfected controls. GAP-43 expression was higher in ACG gray matter (**b**, **c**) and ACG white matter (**e**, **f**) compared to uninfected controls (**a**, **d**, respectively). GAP-43 expression was higher in the hippocampal OML (**h**, **i**) and PUT (**k**, **l**) in SIV-infected rhesus with and without cART compared to uninfected controls (**g**, **j**, respectively). Chromogen is DAB with hematoxylin counterstain. **a**–**c** Original magnification ×200; **d**–**f** original magnification ×80; **g**–**i** original magnification ×20; **j**–**k** original magnification ×40

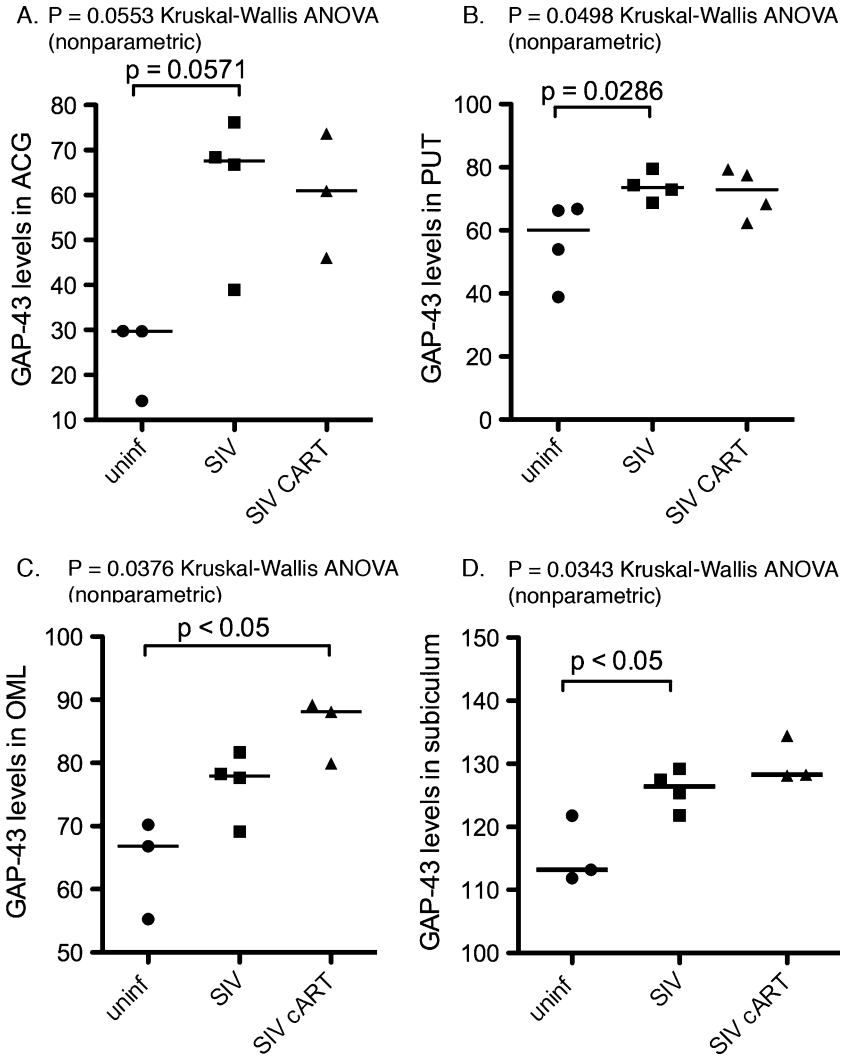

Fig. 4 Computer-aided image analysis of GAP-43. Levels of GAP-43 immunoreactivity in anterior cingulate gyrus (*ACG*), dorsal putamen (*PUT*), outer molecular layer (*OML*), and subiculum were higher in SIV-infected animals with and without cART compared to uninfected controls. Animals that received cART had significantly higher GAP-43 expression in the fibers in the OML (Kruskal–Wallis ANOVA $p=0.0375$, Dunn's post-comparison test $p<0.05$) and an increasing trend in the subiculum (Kruskal–Wallis ANOVA $p=0.0343$) compared to untreated infected and uninfected control animals. Data represent mean levels of GAP-43 expression from 6–10 non-overlapping regions of interest collected at ×80 magnification

by image analysis (Kruskal–Wallis nonparametric $p=0.0376$, Dunn's post-comparison test $p<0.05$, Fig. 4c). There was no significant change in the hippocampal IML (data not shown). Processes in the OML originate from neurons in the entorhinal cortex (EC) and course through the presubiculum and subiculum. GAP-43 expression in the perforant pathway of the presubiculum and subiculum was significantly higher in the SIV-infected animals compared to uninfected controls (Kruskal–Wallis nonparametric ANOVA $p=0.0343$, Dunn's post-comparison test $p<0.05$, Fig. 4d).

GAP-43 mRNA expression is induced in cortex and hippocampus in SIV-infected rhesus macaque

To assess alterations in GAP-43 mRNA expression in response to SIV infection and short-term cART, snap-frozen specimens from frontal cortex, putamen, and hippocampus from the same animals were analyzed by real-time RT-PCR and measured as fold change compared to the uninfected controls. Access to frozen FC samples from CD8-depleted uninfected animals permitted analysis, which demonstrated no significant difference in GAP-43 mRNA between CD8-depleted and non-depleted uninfected animals (Fig. 5a). GAP-43 mRNA differed significantly in the frontal cortex and putamen between the groups of animals (Kruskal–Wallis ANOVA, $p=0.0082$ and 0.0308, respectively; Fig. 5a and b). In the frontal cortex, GAP-43 mRNA was significantly higher in SIV-infected animals with cART compared to uninfected controls (post-analysis Dunn's multicomparison test $p<0.05$; Fig. 5a), while GAP-43 mRNA was nearly twofold lower in SIV-infected treated and untreated rhesus compared to controls (post-analysis Dunn's multicomparison test $p<0.05$; Fig. 5b). In the hippocampus, GAP-43 mRNA mean fold changes were 1.71 and 1.88 in the SIV-infected untreated and cART groups, respectively, compared to uninfected controls, with differences in the cART group approaching significance (unpaired two-tailed *t* test, $p=0.0571$).

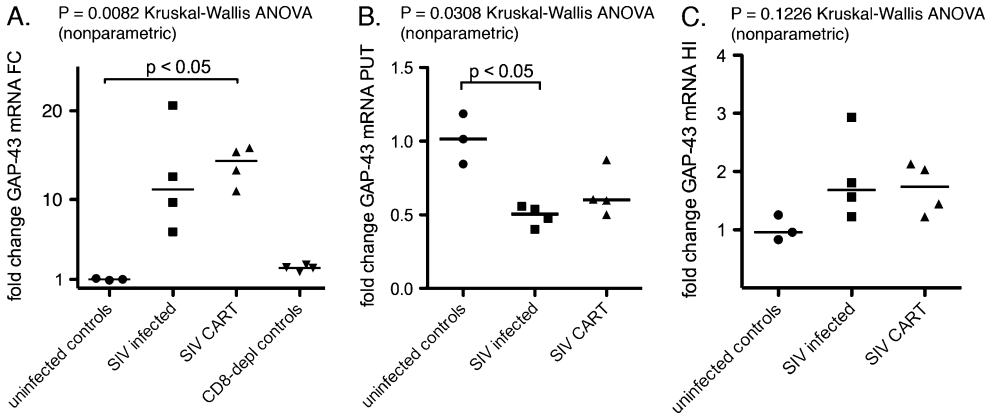

Fig. 5 Quantification of GAP-43 mRNA by quantitative real-time RT-PCR represented as fold change compared to uninfected controls set at 1. In SIV-infected animals, GAP-43 mRNA was significantly higher in frontal cortex (**a**, *FC*, Kruskal–Wallis ANOVA p=0.0082, Dunn's post-comparison test p<0.05 between cART and control groups) and tended toward higher levels in the hippocampus (**c**, *HI*), but was significantly lower in the dorsal putamen (**b**, *PUT*, Kruskal–Wallis ANOVA p= 0.0308, Dunn's post-comparison test p<0.05 between SIV untreated and control groups). There was no significant difference in GAP-43 mRNA levels between CD8-depleted and non-depleted uninfected animals (**a**)

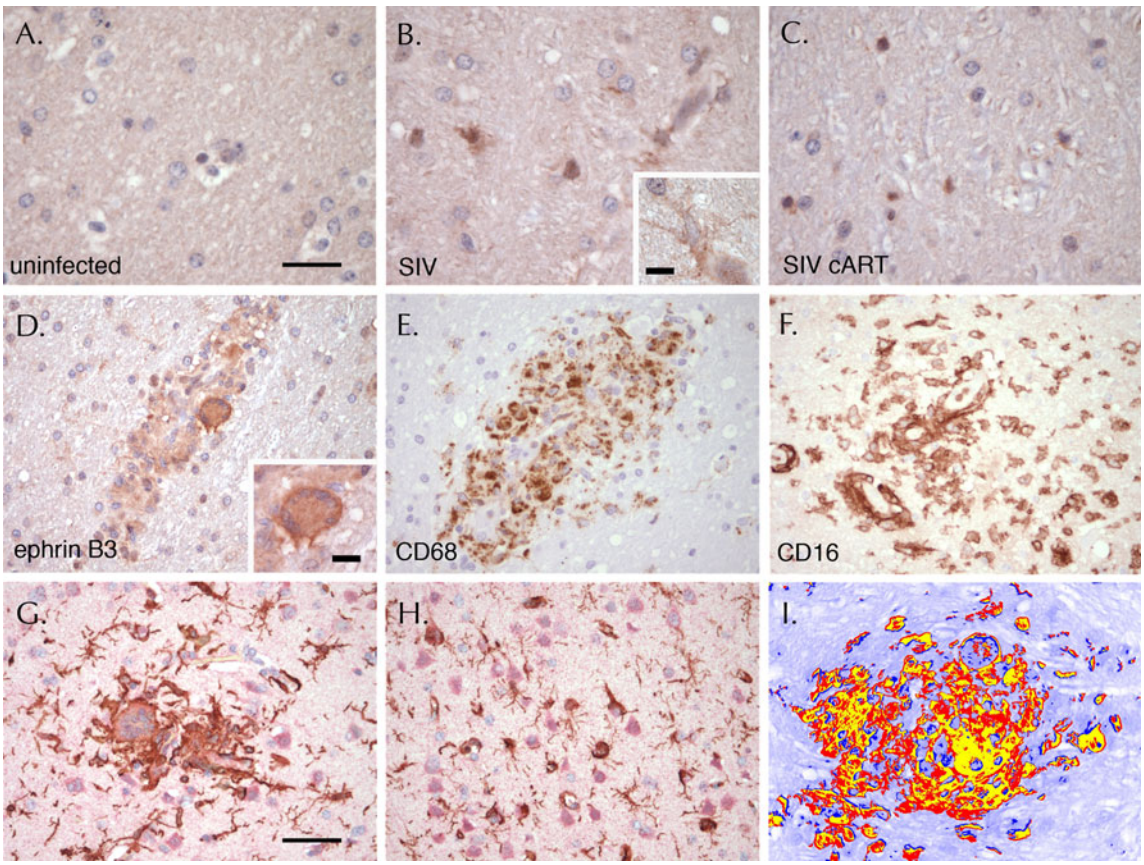

Fig. 6 Ephrin B3, CD68, and CD16 immunohistochemistry in cortex from rhesus macaques. Glial cells morphologically consistent with microglia expressed more ephrin B3 in SIV-infected animals (**b**) and SIV-infected animals that received cART (**c**) compared to uninfected controls (**a**). Perivascular macrophages, multinucleated giant cells, and parenchymal microglia in SIV-infected untreated rhesus express abundant ephrin B3 (**d**), CD68 (**e**), and CD16 (**f**). Double-label immunohistochemistry for Iba-1 positive (DAB, *brown*) and ephrin B3 positive (*permanent red*) perivascular macrophages, multinucleated giant cells and parenchymal microglia (**g**) and large pyramidal neurons in frontal neocortical layer III (**h**) in brain sections from SIV-infected rhesus macaque (**g**). Double-label immunohistochemistry converted to pseudocolorized spectral image of perivascular lesion in SIV-infected rhesus brain with ephrin B3 expression (*blue*) in Iba-1 positive (*red*) macrophages (coexpression is *yellow*). Formalin-fixed paraffin embedded tissue. Mayer's hematoxylin counterstain. **a**–**c** ×80 original magnification (micrometer bar=20 μm); **b** *inset* ×200 original magnification (micrometer bar=10 μm); **d**–**i** ×40 original magnification (micrometer bar=10 μm); **d** inset ×100 original magnification (micrometer bar=5 μm)

Microglial/macrophage expression of ephrin B3 is increased in SIV-infected rhesus

To analyze a possible trigger for increased GAP-43, we analyzed expression of ephrin B3, an important axonal guidance molecule, within resident microglia. Animals in the SIV-infected untreated group had numerous perivascular lesions in neocortical gray and white matter comprised of infiltrating CD68+ (Fig. 6e) and CD16+ (Fig. 6f) macrophages with frequent multinucleated giant cells characteristic of SIV encephalitis. There were few or no infiltrates with no multinucleated giant cells in the SIV-infected animals that received cART (Annamalai et al. 2010; Williams et al. 2005). The cells within the perivascular lesions in the untreated SIV-infected group expressed abundant ephrin B3 (Fig. 6d). In addition, parenchymal cells morphologically consistent with resident microglia within the gray and white matter of frontal cortex of untreated and cART-treated SIV-infected animals (Fig. 6b and c, respectively), also expressed higher ephrin B3 compared to uninfected control animals (Fig. 6a). Macrophages, multinucleated giant cells, and microglia were confirmed as the source of the ephrin B3 with double-label immunohistochemistry with the macrophage-lineage marker Iba-1 (Fig. 6g–i). The majority of the infiltrating, perivascular, Iba-1+ macrophages (Fig. 6g, DAB) expressed abundant cytoplasmic and surface ephrin B3 (Fig. 6g, permanent red) with colocalization of the two proteins set as yellow in the pseudocolorized spectral image (Fig. 6i). In addition, Iba-1 and ephrin B3 co-expressing resident microglia in the gray matter of the frontal cortex are evident encircling large pyramidal, ephrin B3-positive neurons (Fig. 6h). Computer-aided image analysis of the microglia confirmed that ephrin B3 levels in frontal cortical white matter were significantly higher in SIV-infected rhesus compared to controls (Kruskal–Wallis ANOVA $p=0.0376$, Dunn's post-comparison test $p<0.05$, Fig. 7).

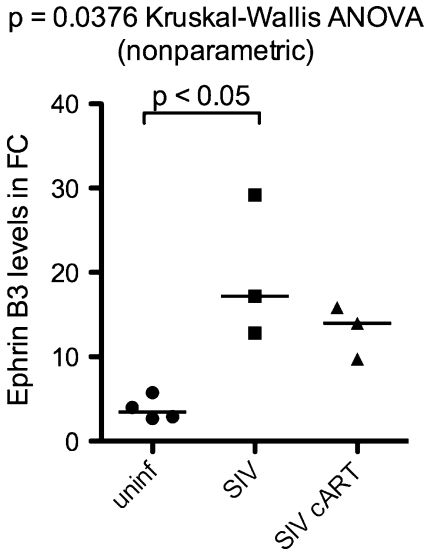

Fig. 7 Computer-aided image analysis of ephrin B3. Ephrin B3 mean levels were higher in SIV-infected animals compared to uninfected controls (Kruskal–Wallis ANOVA $p=0.0376$) with significant difference in SIV-infected animals that did not receive cART (post-comparison Dunn's nonparametric t test $p<0.05$)

Discussion

In this study, we demonstrate that endogenous neuronal repair mechanisms are triggered in adult rhesus macaques in an accelerated SIV-macaque model of HIVE. We report that compromised neuronal metabolism improves in response to short-term cART, reflected by significantly higher terminal NAA/Cr ratios in treated animals compared to untreated SIV-infected animals. We also demonstrate that endogenous neuronal repair processes are triggered in select brain regions in the adult SIV-infected macaque, including induction of GAP-43 and ephrin B3, proteins implicated in neuroadaptation and axonal growth. In particular, we show that there are regional differences in these repair processes, highlighted by upregulation of GAP-43 and synaptic remodeling in specific subregions of the hippocampus.

Our studies suggest that GAP-43 mRNA and protein induction precedes detectable synaptogenesis and remodeling and improvement of neuronal metabolism. Although synaptic density was decreased in multiple brain regions in the SIV-infected rhesus, GAP-43 protein expression was increased in cortical ACG, PUT (a region containing the afferent cortical fibers predominantly from the frontal and parietal neocortices), and HI OML. The only region examined, however, where increases in GAP-43 expression were significantly higher in the cART group was in the hippocampal OML. In the OML, the increase in GAP-43 expression coincided with an increase in mean synaptic density as well, suggesting that in this region increased GAP-43 is associated with synaptic and structural remodeling. The ACG and PUT exhibited persistent lower synaptic density despite increased GAP-43, suggesting the increased in GAP-43 may precede structural and synaptic remodeling. This regional difference in synaptic remodeling may be due to higher intrinsic plasticity in the hippocampus compared to other brain regions. This is further evidenced by the differences in GAP-43 expression in the IML and OML of the hippocampal formation, regions which represent two different neural systems with processes in the IML originating from neurons in the hilus and dentate gyrus granule cell layer while processes in the OML originate from layers II and III of the EC tracking through the subiculum. GAP-43 upregulation with SIV infection was observed in the EC and subiculum in parallel with increases

in the OML, but consistent changes in GAP-43 expression were not evident in the hilus, GCL, or IML. These changes in the hippocampal OML and EC, areas important for learning and memory, likely contribute to the improved cognitive function of HIV patients on HAART.

In addition, we demonstrate that microglia and infiltrating macrophages activated during SIV-infection express the axonal guidance molecule ephrin B3. This observation is supported by previous reports that ephrin B3 and its receptors are expressed by peripheral T lymphocytes and monocytes/macrophages (Yu et al. 2003). Ephrin B3 is a ligand for EphA4 and EphB3 receptors, expressed by neurons and astrocytes (Carmona et al. 2009; Filosa et al. 2009), and is involved in anti-apoptotic activity in neurons (Furne et al. 2009), synapse and dendritic spine formation (Filosa et al. 2009; Klein 2009), and maintenance of axonal stability (Filosa et al. 2009; Klein 2009). Ephrin B3 can also regulate axonal sprouting, and has been associated with induction of GAP-43 (Liu et al. 2006). This suggests a mechanism whereby ephrin B3 expressed by macrophages and microglia could modulate neuron and astrocyte function, as both of these target cells express the ephrin B3 receptors, EphA4 and EphB3 (Carmona et al. 2009; Filosa et al. 2009).

GAP-43 mRNA is induced by nerve growth factor (NGF) (Irwin et al. 2002, 2006). We propose a model whereby microglia and macrophages activated by viral infection express ephrin B3 and stimulate astrocytes, mediated through EphA4 or EphB3, to secrete NGF, which induces GAP-43 in neurons. Other ephrins in addition to ephrin B3 and their receptors are likely involved in this multicellular activation and signaling pathway.

Until now, there has been limited morphological evidence for the improved cognitive state of HIV patients on HAART. This is our first attempt to identify regions and neural pathways that may contribute to improvement of neuronal function on HAART. Additional studies using this SIV-macaque model at additional timepoints post-SIV inoculation will delineate the temporal sequence of ephrin/Eph activation, NGF release, GAP-43 upregulation, and SYN induction in the entorhinal–hippocampal network and cortex. Targeted therapeutic modulation of these extracellular axonal growth molecules, their receptors, and downstream signaling elements may enhance post-injury synaptic remodeling and improve neuronal function. Overall, GAP-43 upregulation in fibers from the cortex, the OML, and the EC reflect a significant potential for synaptic remodeling, regeneration, and repair in the adult primate brain.

Acknowledgments We would like to thank Dr. Larry Benowitz for supplying the anti- GAP-43 antibody and protocol, Ron Desrosiers for supplying the virus inoculum SIVmac251, Keith Reimann for providing anti-CD8 cM-T807, Raymond Schinazi for supplying Racivir (RCV), and Norbert Bischofberger of Gilead Sciences for providing PMPA. In addition, we thank Elizabeth Curran, Michael O'Connell, and Doug Pauley for pathology assistance, and Drs. Prabhat Sehgal, Angela Carville, and Elisabeth Moeller for veterinary expertise. We also thank Hayley Dirscherl, Alexis Denysyk, Heather Knight, and Karen Boisvert Dalecki for their contribution with immunohistochemistry and Hong Yang for real-time PCR contribution. This work was supported by RR00168 (NEPRC Base Grant), R01NS050041 (RGG), DA025697 (GMM), and the NEPRC Microscopy and Primate Genetics Cores.

References

Alirezaei M, Watry DD, Flynn CF, Kiosses WB, Masliah E, Williams BR, Kaul M, Lipton SA, Fox HS (2007) Human immunodeficiency virus-1/surface glycoprotein 120 induces apoptosis through RNA-activated protein kinase signaling in neurons. J Neurosci 27:11047–11055

Annamalai L, Bhaskar V, Pauley DR, Knight H, Williams K, Lentz M, Ratai E, Westmoreland SV, Gonzalez RG, O'Neil SP (2010) Impact of short-term combined antiretroviral therapy on brain virus burden in simian immunodeficiency virus-infected and CD8+ lymphocyte-depleted rhesus macaques. Am J Pathol 177:777–791

Benowitz LI, Routtenberg A (1997) GAP-43: an intrinsic determinant of neuronal development and plasticity. Trends Neurosci 20: 84–91

Benowitz LI, Apostolides PJ, Perrone-Bizzozero N, Finklestein SP, Zwiers H (1988) Anatomical distribution of the growth-associated protein GAP-43/B-50 in the adult rat brain. J Neurosci 8:339–352

Benowitz LI, Perrone-Bizzozero NI, Finklestein SP, Bird ED (1989) Localization of the growth-associated phosphoprotein GAP-43 (B-50, F1) in the human cerebral cortex. J Neurosci 9:990–995

Benowitz LI, Perrone-Bizzozero NI, Neve RL, Rodriguez W (1990a) GAP-43 as a marker for structural plasticity in the mature CNS. Prog Brain Res 86:309–320

Benowitz LI, Rodriguez WR, Neve RL (1990b) The pattern of GAP-43 immunostaining changes in the rat hippocampal formation during reactive synaptogenesis. Brain Res Mol Brain Res 8: 17–23

Benson MD, Romero MI, Lush ME, Lu QR, Henkemeyer M, Parada LF (2005) Ephrin-B3 is a myelin-based inhibitor of neurite outgrowth. Proc Natl Acad Sci U S A 102:10694–10699

Bissel SJ, Wang G, Ghosh M, Reinhart TA, Capuano S 3rd, Stefano Cole K, Murphey-Corb M, Piatak M Jr, Lifson JD, Wiley CA (2002) Macrophages relate presynaptic and postsynaptic damage in simian immunodeficiency virus encephalitis. Am J Pathol 160:927–941

Carmichael ST, Archibeque I, Luke L, Nolan T, Momiy J, Li S (2005) Growth-associated gene expression after stroke: evidence for a growth-promoting region in peri-infarct cortex. Exp Neurol 193:291–311

Carmona MA, Murai KK, Wang L, Roberts AJ, Pasquale EB (2009) Glial ephrin-A3 regulates hippocampal dendritic spine morphology and glutamate transport. Proc Natl Acad Sci U S A 106:12524–12529

Chumley MJ, Catchpole T, Silvany RE, Kernie SG, Henkemeyer M (2007) EphB receptors regulate stem/progenitor cell proliferation,

migration, and polarity during hippocampal neurogenesis. J Neurosci 27:13481–13490
Everall IP, Trillo-Pazos G, Bell C, Mallory M, Sanders V, Masliah E (2001) Amelioration of neurotoxic effects of HIV envelope protein gp120 by fibroblast growth factor: a strategy for neuroprotection. J Neuropathol Exp Neurol 60:293–301
Everall IP, Bell C, Mallory M, Langford D, Adame A, Rockestein E, Masliah E (2002) Lithium ameliorates HIV-gp120-mediated neurotoxicity. Mol Cell Neurosci 21:493–501
Filosa A, Paixao S, Honsek SD, Carmona MA, Becker L, Feddersen B, Gaitanos L, Rudhard Y, Schoepfer R, Klopstock T, Kullander K, Rose CR, Pasquale EB, Klein R (2009) Neuron-glia communication via EphA4/ephrin-A3 modulates LTP through glial glutamate transport. Nat Neurosci 12:1285–1292
Fox HS, Weed MR, Huitron-Resendiz S, Baig J, Horn TF, Dailey PJ, Bischofberger N, Henriksen SJ (2000) Antiviral treatment normalizes neurophysiological but not movement abnormalities in simian immunodeficiency virus-infected monkeys. J Clin Invest 106:37–45
Furne C, Ricard J, Cabrera JR, Pays L, Bethea JR, Mehlen P, Liebl DJ (2009) EphrinB3 is an anti-apoptotic ligand that inhibits the dependence receptor functions of EphA4 receptors during adult neurogenesis. Biochim Biophys Acta 1793:231–238
Gonzalez RG, Cheng LL, Westmoreland SV, Sakaie KE, Becerra LR, Lee PL, Masliah E, Lackner AA (2000) Early brain injury in the SIV-macaque model of AIDS. AIDS 14:2841–2849
Greco JB, Westmoreland SV, Ratai EM, Lentz MR, Sakaie K, He J, Sehgal PK, Masliah E, Lackner AA, Gonzalez RG (2004) In vivo 1H MRS of brain injury and repair during acute SIV infection in the macaque model of neuroAIDS. Magn Reson Med 51:1108–1114
Gupta RG, Kelly KM, Helke KL, Queen SE, Karper JM, Dorsey JL, Brice AK, Adams RJ, Tarwater PM, Kolson DL, Mankowski JL (2010) HIV and SIV induce alterations in CNS CaMKII expression and activation: a potential mechanism for cognitive impairment. Am J Pathol 176:2776–2784
Haworth SJ, Christofalo B, Anderson RD, Dunkle LM (1998) A single-dose study to assess the penetration of stavudine into human cerebrospinal fluid in adults. J Acquir Immune Defic Syndr Hum Retrovirol 17:235–238
Higo N, Nishimura Y, Murata Y, Oishi T, Yoshino-Saito K, Takahashi M, Tsuboi F, Isa T (2009) Increased expression of the growth-associated protein 43 gene in the sensorimotor cortex of the macaque monkey after lesioning the lateral corticospinal tract. J Comp Neurol 516:493–506
Irwin N, Chao S, Goritchenko L, Horiuchi A, Greengard P, Nairn AC, Benowitz LI (2002) Nerve growth factor controls GAP-43 mRNA stability via the phosphoprotein ARPP-19. Proc Natl Acad Sci U S A 99:12427–12431
Irwin N, Li YM, O'Toole JE, Benowitz LI (2006) Mst3b, a purine-sensitive Ste20-like protein kinase, regulates axon outgrowth. Proc Natl Acad Sci U S A 103:18320–18325
Jacobson RD, Virag I, Skene JH (1986) A protein associated with axon growth, GAP-43, is widely distributed and developmentally regulated in rat CNS. J Neurosci 6:1843–1855
Klein R (2009) Bidirectional modulation of synaptic functions by Eph/ephrin signaling. Nat Neurosci 12:15–20
Lentz MR, Kim JP, Westmoreland SV, Greco JB, Fuller RA, Ratai EM, He J, Sehgal PK, Halpern EF, Lackner AA, Masliah E, Gonzalez RG (2005) Quantitative neuropathologic correlates of changes in ratio of N-acetylaspartate to creatine in macaque brain. Radiology 235:461–468
Lentz MR, Westmoreland SV, Lee V, Ratai EM, Halpern EF, Gonzalez RG (2008) Metabolic markers of neuronal injury correlate with SIV CNS disease severity and inoculum in the macaque model of neuroAIDS. Magn Reson Med 59:475–484
Lipton SA, Brenneman DE, Silverstein FS, Masliah E, Mucke L (1995) gp120 and neurotoxicity in vivo. Trends Pharmacol Sci 16:122
Liu X, Hawkes E, Ishimaru T, Tran T, Sretavan DW (2006) EphB3: an endogenous mediator of adult axonal plasticity and regrowth after CNS injury. J Neurosci 26:3087–3101
Masliah E, Achim CL, Ge N, DeTeresa R, Terry RD, Wiley CA (1992a) Spectrum of human immunodeficiency virus-associated neocortical damage. Ann Neurol 32:321–329
Masliah E, Ge N, Achim CL, Hansen LA, Wiley CA (1992b) Selective neuronal vulnerability in HIV encephalitis. J Neuropathol Exp Neurol 51:585–593
Masliah E, Ge N, Morey M, DeTeresa R, Terry RD, Wiley CA (1992c) Cortical dendritic pathology in human immunodeficiency virus encephalitis. Lab Invest 66:285–291
Masliah E, Heaton RK, Marcotte TD, Ellis RJ, Wiley CA, Mallory M, Achim CL, McCutchan JA, Nelson JA, Atkinson JH, Grant I (1997) Dendritic injury is a pathological substrate for human immunodeficiency virus-related cognitive disorders. HNRC Group. The HIV Neurobehavioral Research Center. Ann Neurol 42:963–972
Neve RL, Finch EA, Bird ED, Benowitz LI (1988) Growth-associated protein GAP-43 is expressed selectively in associative regions of the adult human brain. Proc Natl Acad Sci U S A 85:3638–3642
Perrone-Bizzozero NI, Weiner D, Hauser G, Benowitz LI (1988) Extraction of major acidic Ca2+ dependent phosphoproteins from synaptic membranes. J Neurosci Res 20:346–350
Ratai EM, Bombardier JP, Joo CG, Annamalai L, Burdo TH, Campbell J, Fell R, Hakimelahi R, He J, Autissier P, Lentz MR, Halpern EF, Masliah E, Williams KC, Westmoreland SV, Gonzalez RG (2010) Proton magnetic resonance spectroscopy reveals neuroprotection by oral minocycline in a nonhuman primate model of accelerated NeuroAIDS. PLoS One 5:e10523
Ratai EM, Pilkenton S, He J, Fell R, Bombardier JP, Joo CG, Lentz MR, Kim WK, Burdo TH, Autissier P, Annamalai L, Curran E, O'Neil SP, Westmoreland SV, Williams KC, Masliah E, Gilberto Gonzalez R (2011) CD8(+) lymphocyte depletion without SIV infection does not produce metabolic changes or pathological abnormalities in the rhesus macaque brain. J Med Primatol. doi:10.1111/j.1600-0684.2011.00475.x
Schinazi RF, Boudinot FD, Ibrahim SS, Manning C, McClure HM, Liotta DC (1992) Pharmacokinetics and metabolism of racemic 2′,3′-dideoxy-5-fluoro-3′-thiacytidine in rhesus monkeys. Antimicrob Agents Chemother 36:2432–2438
Schmitz JE, Kuroda MJ, Santra S, Sasseville VG, Simon MA, Lifton MA, Racz P, Tenner-Racz K, Dalesandro M, Scallon BJ, Ghrayeb J, Forman MA, Montefiori DC, Rieber EP, Letvin NL, Reimann KA (1999) Control of viremia in simian immunodeficiency virus infection by CD8+ lymphocytes. Science 283:857–860
Strittmatter SM, Vartanian T, Fishman MC (1992) GAP-43 as a plasticity protein in neuronal form and repair. J Neurobiol 23:507–520
Westmoreland SV, Kolson D, Gonzalez-Scarano F (1996) Toxicity of TNF alpha and platelet activating factor for human NT2N neurons: a tissue culture model for human immunodeficiency virus dementia. J Neurovirol 2:118–126
Westmoreland SV, Alvarez X, deBakker C, Aye P, Wilson ML, Williams KC, Lackner AA (2002) Developmental expression patterns of CCR5 and CXCR4 in the rhesus macaque brain. J Neuroimmunol 122:146–158
Wiley CA, Masliah E, Morey M, Lemere C, DeTeresa R, Grafe M, Hansen L, Terry R (1991) Neocortical damage during HIV infection. Ann Neurol 29:651–657

Williams K, Westmoreland S, Greco J, Ratai E, Lentz M, Kim WK, Fuller RA, Kim JP, Autissier P, Sehgal PK, Schinazi RF, Bischofberger N, Piatak M, Lifson JD, Masliah E, Gonzalez RG (2005) Magnetic resonance spectroscopy reveals that activated monocytes contribute to neuronal injury in SIV neuroAIDS. J Clin Invest 115:2534–2545

Xie Z, Westmoreland SV, Bahn ME, Chen GL, Yang H, Vallender EJ, Yao WD, Madras BK, Miller GM (2007) Rhesus monkey trace amine-associated receptor 1 signaling: enhancement by monoamine transporters and attenuation by the D2 autoreceptor in vitro. J Pharmacol Exp Ther 321:116–127

Xu NJ, Henkemeyer M (2009) Ephrin-B3 reverse signaling through Grb4 and cytoskeletal regulators mediates axon pruning. Nat Neurosci 12:268–276

Yu G, Luo H, Wu Y, Wu J (2003) Mouse ephrinB3 augments T-cell signaling and responses to T-cell receptor ligation. J Biol Chem 278:47209–47216